Politeknik Dergisi
Cilt: 10 Sayı: 2 s. 163-171, 2007

Journal of Polytechnic
Vol: 10 No: 2 pp. 163-171, 2007

The Effect of Square Hole on Thermal Stresses in an Aluminum Metal-Matrix Cross-Ply Laminated Composites

Faruk ŞEN
Dokuz Eylul University Department of Mechanical Engineering
35100 Bornova, İZMİR

ABSTRACT

In this study, the effect of a square hole on thermal stresses in a cross ply laminated composite plates reinforced steel fiber-aluminum metal-matrix was examined. Laminated composite plates were composed of four orthotropic layers. The stacking sequences of composite were also selected as symmetric $(0/90)_s$ and antisymmetric $(0/90)_2$ manners. Uniform temperature distribution was selected as thermal loading. Finite element method (FEM) was performed to calculate the magnitude of the thermal stresses, ANSYS software was used during the solution. The width square laminated plate-to-the square hole dimension, a/b, was chosen as 5. The results were given in graphical forms.

Keywords: Thermal stresses, finite element method, laminated composites

Çapraz Takviye Edilmiş Alüminyum Matriksli Tabakalı Kompozitlerde Kare Deliğin Isıl Gerilmeler Üzerindeki Etkisi

ÖZET

Bu çalışmada, alüminyum matriksli çelik tellerle çapraz olarak takviye edilmiş kompozit plaklarda meydana gelen ısıl gerilmeler üzerine, bir kare deliğin etkisi incelenmiştir. Tabakalı kompozit plakalar, dört farklı tabakacığın birleştirilmesi ile meydana getirilmiştir. Tabakaların dizilişi, simetrik $(0/90)_s$ ve antisimetrik $(0/90)_2$ biçimde düzenlenmiştir. Isıl yük olarak çeşitli değerlerde homojen sıcaklık dağılımları seçilmiştir. Isıl gerilme değerlerinin hesaplanması için sonlu elemanlar metodu uygulanmıştır, bunun için çözümde ANSYS yazılımı kullanılmıştır. Tabakalı kompozit levhanın genişliğinin, kare deliğin boyutlarına oranı olan a/b, 5 olarak seçilmiştir. Sonuçlar şekillerde gösterilmiştir.

Anahtar Kelimeler: Isıl gerilmeler, sonlu elemanlar metodu, tabakalı kompozitler

1. INTRODUCTION

Metal-matrix composites are superior for their performance at elevated temperatures compared to glass-reinforced plastics. The strength and elastic moduli of metal matrices are higher than those resin matrices over a wide range of temperature. As to deformation of the composites metal matrices can greatly enhance the ductility of the composite. The stress concentrations reduced by cracked fibers can be relaxed through the plastic deformation of matrix. As a result there is a less chance of a brittle failure of the composite (1).

A thermal elastic–plastic stress analysis was carried out on symmetric steel fiber aluminum metal matrix composite laminated plates fixed at all edges. An analytical solution was performed and temperatures vary linearly along the thickness of the plates (2). An elastic-plastic thermal stress analysis was performed on steel-fibre-reinforced aluminum-matrix composite beams. The temperature takes the values zero and T_0 at the upper–lower surfaces and on the middle axis, respectively, and it was selected to vary parabolically (3).

Residual stress analysis of laminated composite plates under thermal loads and temperature change also through the thickness of plates were studied using analytical methods (4). A thermal elastic-plastic stress analysis was carried out on a steel fibre high density polyethylene matrix composite beam. The distribution of residual stress and deformations in the beam were obtained for the case that the temperature distribution varies linearly between the upper and lower surfaces (5). An investigation was performed to study the response of a thermal elasto-plastic stress analysis and residual stresses on symmetric cross ply and angle–ply, steel fiber reinforced thermoplastic laminated plate, which was subjected to a uniform temperature load with a circular hole (6).

Digital Object Identifier 10.2339/2007.10.2.163-171

In this study, a thermal stress analysis was performed on symmetric and antisymmetric cross ply steel fiber reinforced aluminum metal-matrix laminated composite plates with a square hole, since the effect of a square hole on thermal stresses was investigated. Finite element method (FEM) was used to solve the thermal stress problem. For this reason, a general purpose finite element program ANSYS was used during the solution. Uniform temperature distribution was selected as thermal loading.

2. MATERIALS AND METHODS

2.1. Statement of the Problem

A steel fiber reinforced aluminum metal-matrix composite material was used in this analysis. Its mechanical properties of the composites were given in Table 1 (7). The dimensions of the square laminated composite plate with a square hole were shown in Fig. 1. As seen in this figure, the length of each edge of plate and square hole were chosen as a=300 mm and b=60 mm, respectively. Thus, a/b ratio was selected as 5. The laminated plate was formed from four layers. The thickness of each layer was 2 mm. Besides, the stacking sequences of laminated composite plates were assumed as symmetric, $(0/90)_s$ and antisymmetric, $(0/90)_2$ manners, this case were also illustrated in Fig. 2. Composite laminated plates were assumed simple supported. Furthermore, because of the stacking sequence of laminates, a quarter part of the whole plate was modeled. Uniform temperature distributions were also selected as thermal loading, variously. It was carried out on each model as 100, 120 and 140 ^{o}C.

Finite element method (FEM) was used to calculate the magnitude of the thermal stresses, so a general purpose finite element code ANSYS was preferred for the solution. During the mesh generation process, SOLID46 element type was selected in ANSYS. The shape and properties of this element type was also shown in Fig. 3. Meanwhile, the boundary conditions and finite element modeling of the composite plate with a square hole were shown in Fig. 4. It is seen that in this figure, mapped mesh form were preferred for finite element modeling. After the mesh generation process, 1392 nodes and 924 elements were created.

2.2 Mathematical Formulation

The three-dimensional thermoelastic anisotropic strain-stress relations are given by Jones as (8),

$$\varepsilon_i = S_{ij}\sigma_j + \alpha_i \Delta T \;\; i,j = 1,2,.....,6 \qquad (1)$$

where, ΔT is the temperature change, ε_i are the mechanical strain components, S_{ij} is the compliance matrix, σ_j are the stress components, α_i are the thermal expansion coefficients of the composite. The three-dimensional stress-strain relations are calculated by inversion:

$$\sigma_i = C_{ij}(\varepsilon_i - \alpha_j \Delta T) \;\; i,j = 1,2,.....,6 \qquad (2)$$

where C_{ij} is the stiffness matrix. In both equations (1) and (2), the six α_i are the coefficients of thermal deformation (expansion or contraction and distortion, i.e., shear), and ΔT is the temperature difference. In equation (2), the terms $C_{ij}\alpha_j \Delta T$ are the thermal stresses if the total strain is zero (8).

Plane stresses of on an orthotropic lamina in principal material coordinates are

$$\begin{bmatrix}\sigma_1\\ \sigma_2\\ \tau_{12}\end{bmatrix} = \begin{bmatrix}Q_{11} & Q_{12} & 0\\ Q_{12} & Q_{22} & 0\\ 0 & 0 & Q_{66}\end{bmatrix}\begin{bmatrix}\varepsilon_1 - \alpha_1\Delta T\\ \varepsilon_2 - \alpha_2\Delta T\\ \gamma_{12}\end{bmatrix} \qquad (3)$$

The stresses in laminate coordinates for the k^{th} layer are computed by transformation of coordinates.

$$\begin{bmatrix}\sigma_x\\ \sigma_y\\ \tau_{xy}\end{bmatrix}_k = \begin{bmatrix}\overline{Q_{11}} & \overline{Q_{12}} & \overline{Q_{16}}\\ \overline{Q_{12}} & \overline{Q_{22}} & \overline{Q_{26}}\\ \overline{Q_{16}} & \overline{Q_{26}} & \overline{Q_{66}}\end{bmatrix}\begin{bmatrix}\varepsilon_x - \alpha_x\Delta T\\ \varepsilon_y - \alpha_y\Delta T\\ \gamma_{xy} - \alpha_{xy}\Delta T\end{bmatrix}_k \qquad (4)$$

The layer stresses are integrated through the thickness, the force resultants are,

$$\begin{bmatrix}N_x\\ N_y\\ N_{xy}\end{bmatrix} = \begin{bmatrix}A_{11} & A_{12} & A_{16}\\ A_{12} & A_{22} & A_{26}\\ A_{16} & A_{26} & A_{66}\end{bmatrix}\begin{bmatrix}\varepsilon_x^o\\ \varepsilon_y^o\\ \gamma_{xy}^o\end{bmatrix} + \begin{bmatrix}B_{11} & B_{12} & B_{16}\\ B_{12} & B_{22} & B_{26}\\ B_{16} & B_{26} & B_{66}\end{bmatrix}\begin{bmatrix}K_x\\ K_y\\ K_{xy}\end{bmatrix} - \begin{bmatrix}N_x^T\\ N_y^T\\ N_{xy}^T\end{bmatrix} \qquad (5)$$

in which the A_{ij} and B_{ij} are the usual extensional and bending-extension coupling stiffness and the thermal forces are

$$\begin{bmatrix}N_x^T\\ N_y^T\\ N_{xy}^T\end{bmatrix} = \int\begin{bmatrix}\overline{Q_{11}} & \overline{Q_{12}} & \overline{Q_{16}}\\ \overline{Q_{12}} & \overline{Q_{22}} & \overline{Q_{26}}\\ \overline{Q_{16}} & \overline{Q_{26}} & \overline{Q_{66}}\end{bmatrix}_k\begin{bmatrix}\alpha_x\\ \alpha_y\\ \alpha_{xy}\end{bmatrix}_k \Delta T dz \qquad (6)$$

In a similar way, the moment resultants are calculated by integrating the moment of the stresses through the thickness (8):

$$\begin{bmatrix}M_x\\ M_y\\ M_{xy}\end{bmatrix} = \begin{bmatrix}B_{11} & B_{12} & B_{16}\\ B_{12} & B_{22} & B_{26}\\ B_{16} & B_{26} & B_{66}\end{bmatrix}\begin{bmatrix}\varepsilon_x^o\\ \varepsilon_y^o\\ \gamma_{xy}^o\end{bmatrix} + \begin{bmatrix}D_{11} & D_{12} & D_{16}\\ D_{12} & D_{22} & D_{26}\\ D_{16} & D_{26} & D_{66}\end{bmatrix}\begin{bmatrix}K_x\\ K_y\\ K_{xy}\end{bmatrix} - \begin{bmatrix}M_x^T\\ M_y^T\\ M_{xy}^T\end{bmatrix} \qquad (7)$$

in which the D_{ij} are the usual bending stiffness and the thermal moments are,

$$\begin{bmatrix}M_x^T\\ M_y^T\\ M_{xy}^T\end{bmatrix} = \int\begin{bmatrix}\overline{Q_{11}} & \overline{Q_{12}} & \overline{Q_{16}}\\ \overline{Q_{12}} & \overline{Q_{22}} & \overline{Q_{26}}\\ \overline{Q_{16}} & \overline{Q_{26}} & \overline{Q_{66}}\end{bmatrix}_k\begin{bmatrix}\alpha_x\\ \alpha_y\\ \alpha_{xy}\end{bmatrix}_k \Delta T dz \qquad (8)$$

Actually, only in the restricted case of perfect constraint are the N^T and M^T thermal forces and moments, respectively. However, the force and moment resultants can be rearranged to read,

$$\begin{bmatrix}\overline{N_x}\\ \overline{N_y}\\ \overline{N_{xy}}\end{bmatrix}=\begin{bmatrix}N_x+N_x^T\\ N_y+N_y^T\\ N_{xy}+N_{xy}^T\end{bmatrix}=\begin{bmatrix}A_{11} & A_{12} & A_{16}\\ A_{12} & A_{22} & A_{26}\\ A_{16} & A_{26} & A_{66}\end{bmatrix}\begin{bmatrix}\varepsilon_x^o\\ \varepsilon_y^o\\ \gamma_{xy}^o\end{bmatrix}+\begin{bmatrix}B_{11} & B_{12} & B_{16}\\ B_{12} & B_{22} & B_{26}\\ B_{16} & B_{26} & B_{66}\end{bmatrix}\begin{bmatrix}K_x\\ K_y\\ K_{xy}\end{bmatrix} \quad (9)$$

$$\begin{bmatrix}\overline{M_x}\\ \overline{M_y}\\ \overline{M_{xy}}\end{bmatrix}=\begin{bmatrix}M_x+M_x^T\\ M_y+M_y^T\\ M_{xy}+M_{xy}^T\end{bmatrix}=\begin{bmatrix}B_{11} & B_{12} & B_{16}\\ B_{12} & B_{22} & B_{26}\\ B_{16} & B_{26} & B_{66}\end{bmatrix}\begin{bmatrix}\varepsilon_x^o\\ \varepsilon_y^o\\ \gamma_{xy}^o\end{bmatrix}+\begin{bmatrix}D_{11} & D_{12} & D_{16}\\ D_{12} & D_{22} & D_{26}\\ D_{16} & D_{26} & D_{66}\end{bmatrix}\begin{bmatrix}K_x\\ K_y\\ K_{xy}\end{bmatrix} \quad (10)$$

in the form of equations (9) and (10), the thermal portion of thermal and mechanical stress problems can be treated as equivalent mechanical loads defined by N^T and M^T in Equations (6) and (8), respectively in addition to the mechanical loads, N and M (8).

The stress components in the principal material directions can be written as,

$$\begin{Bmatrix}\sigma_1\\ \sigma_2\\ \tau_{12}\end{Bmatrix}=\begin{bmatrix}\cos^2 & \sin^2 & 2\sin\cos\\ \sin^2 & \cos^2 & -2\sin\cos\\ -\sin\cos & \sin\cos & \cos^2-\sin^2\end{bmatrix}\begin{Bmatrix}\sigma_x\\ \sigma_y\\ \tau_{xy}\end{Bmatrix} \quad (11)$$

3. RESULTS AND DISCUSSION

Thermal stress distributions are calculated as same both upper and lower surfaces of the symmetric manner, whereas its distributions on upper and lower surfaces of antisymmetric manner are obtained differ from each other. Therefore, thermal stress distributions on lower surface of symmetric manner are not shown in results, while its distributions are illustrated for both upper and lower surfaces of antisymmetric manner, separately. Thermal stress distributions are illustrated both symmetric $(0/90)_s$ and upper surface of antisymmetric $(0/90)_2$ manners for x and y directions in Figs. 5 and 6, respectively. In these figures, it is also plotted depending on applied different uniform thermal loadings which are mentioned above as 100, 120 and 140 ^oC. It is seen that in these figures, absolute value of thermal stresses are increased related to rise of applied uniform temperature loading. Therefore, the maximum values of it are calculated at 140 ^oC both symmetric and antisymmetric manner. For example, the maximum values of σ_x are computed 10,792 MPa as tensile and 10,903 MPa as compressive for symmetric manner, although it is obtained 11,259 MPa as tensile and 11,276 MPa as compressive on upper surface of antisymmetric manner in Figure 5. In addition, the maximum values of σ_y are calculated 10,903 MPa as tensile and 10,792 MPa as compressive for symmetric manner, even though it is estimated 11,958 MPa as tensile and 11,873 MPa as compressive on upper surface of antisymmetric manner in Figure 6. Another important point from these figures, thermal stress values for antisymmetric manner are higher than symmetric manner. Additionally, the maximum absolute value of thermal stresses for symmetric manner are the same both x and y-directions, but the maximum absolute value of it for y-direction is higher than x-direction for antisymmetric manner.

Thermal shear stress distributions of symmetric and upper surface of antisymmetric manners at different thermal loadings are shown in Fig. 7. It is seen that in this figure, the magnitude of thermal shear stresses for symmetric manner are higher than upper surface of antisymmetric manner as tensile form, nevertheless the magnitude of it for upper surface of antisymmetric manner is greater than symmetric manner as compressive form. Furthermore, thermal shear stresses which are calculated for symmetric manner as compressive are very small values if to compare with antisymmetric manner results, so these values can be neglected.

As mentioned previously, thermal stress distributions on upper and lower surfaces of cross ply anstisymmetric laminated composites are estimated differ from each other, so thermal stress distributions on lower surface are also illustrated in Fig. 8 for x and y-directions. It is seen in this Figure, thermal stress distributions are plotted depending on applied uniform temperature loadings. The maximum value of thermal stresses for lower surface of antisymmetric manner is calculated 11,958 MPa as tensile form at 140 ^oC for y-direction.

If all figures are investigated carefully, it can be clearly seen that, the distributions of thermal stresses are very high concentrated around the square hole of the laminated composite plates. For this reason, it is said that the square hole effected thermal stress distributions very strictly. Meanwhile the corner of the square hole may cause crack propagation because of the intensity of the thermal stresses on this part of the plate.

4. CONCLUSIONS

According to the present study results, the following points are concluded that;

1. Due to the high thermal stress concentration around the square hole, it can be said that thermal stress distributions are effected from the square hole, obviously.
2. The magnitudes of the thermal stresses increase related to rise of uniform temperature loadings, therefore the highest value of it is computed at 140 °C.
3. Whereas the thermal stress distributions on the upper and lower layers of the symmetric manner are the same, the stress distributions of them are differing from each other for antisymmetric manner.
4. The absolute values of thermal normal stresses for the symmetric cross-ply laminated plates are obtained lower than antisymmetrically laminated plates for all uniform temperatures.

REFERENCES

1. Ataberk, N., Uyaner, M., Avcı, A., Koçak, S., Elasto-plastic Stress Analysis of Aluminum Metal-Matrix Composite Plate Under In-Plane Loading, Journal of Reinforced Plastics and Composites, 23, 563-570, 2004.
2. Sayman O., Elastic–plastic Stress Analysis of Symmetric Aluminum Metal-matrix Composite Laminated Plates under Thermal Loads Varying Linearly, Composites Part B: Engineering, 36, 61-72, 2005.
3. Sayman O., Özer, M.R., Elastic–Plastic Thermal Stress Analysis of Aluminum-Martix Composite Beams Under a Parabolically Temperature Distribution, Composites Science and Technology, 61, 2129-2137, 2001.
4. Senel, M., Akbulut, H., and Toparli, M., Residual Stress Analysis in Symmetric Thermoplastic Laminated Plates Under Thermal Loads: Analytic Solution Journal of Thermoplastic Composite Materials, 17, 481-507, 2004.
5. Sayman, O., Karakuzu, R., Daghan, B. and Kocak S., Elastic-Plastic Stress Analysis of Thermoplastic Composite Beams under Temperature Distributed Linearly, Journal of Thermoplastic Composite Materials, 15, 193-208, 2002.
6. Şen, F., An Investigation of Thermal Elasto-Plastic Stress Analysis of Laminated Thermoplastic Composites with a Circular Hole under Uniform Temperature Loading, Science and Engineering of Composite Materials, 13, 213-224, 2006.
7. Sayman, O., Elastic-Plastic and Residual Stresses in Symmetric Aluminum Metal-Matrix Laminated Plates Under a Linear Thermal Loading, Journal of Thermal Stresses, 26, 391-406, 2003.
8. Jones, R.M., Mechanics of Composite Materials. Taylor & Francis Inc. USA, 1999.

TABLES

Table 1. Mechanical properties of the composite material (7)

E_1 (MPa)	E_2 (MPa)	G_{12} (MPa)	ν_{12}	α_1 (1/°C)	α_2 (1/°C)
85000	74000	30000	0,29	$18,5x10^{-6}$	$21x10^{-6}$

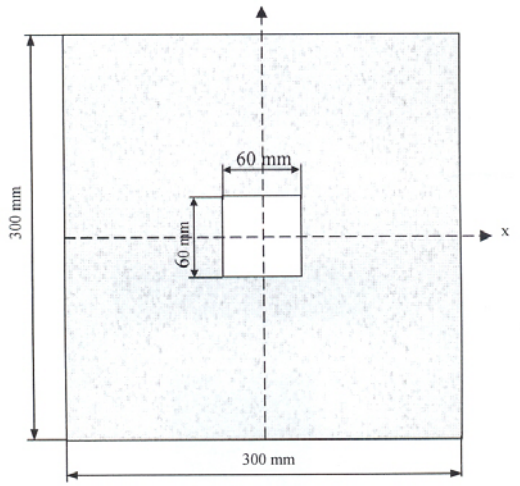

Figure 1. The dimensions of composite plate with a square hole

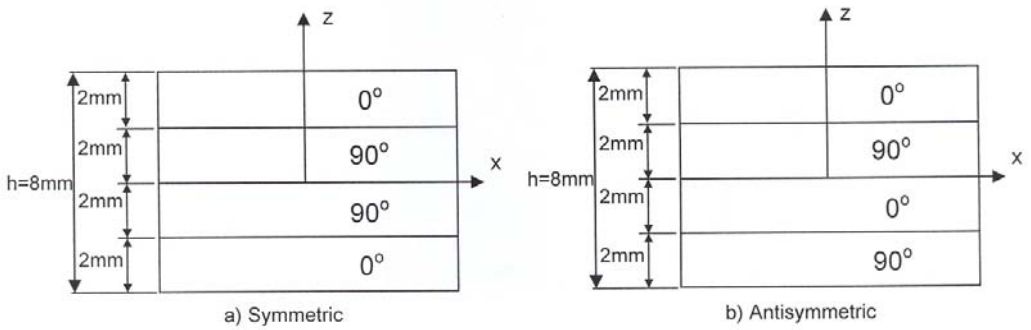

Figure 2. Stacking sequence of laminated composite plates

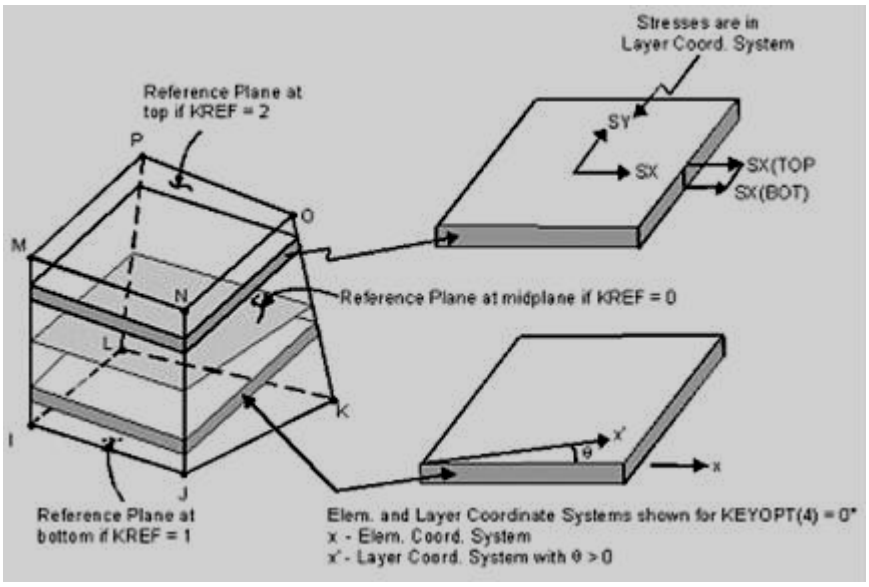

Figure 3. SOLID46 element type in ANSYS

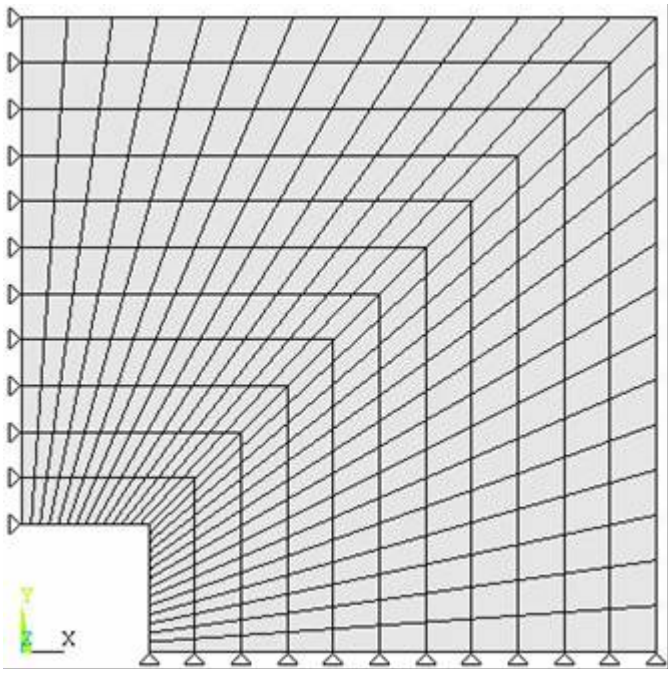

Figure 4. The boundary conditions and finite element modeling

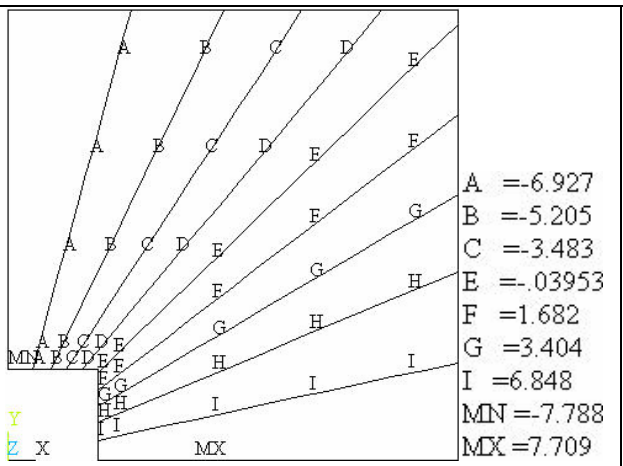

a) 100 °C

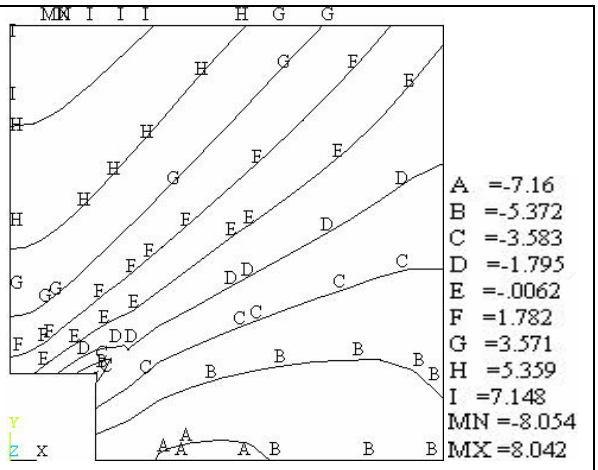

a) 100 °C, upper surface

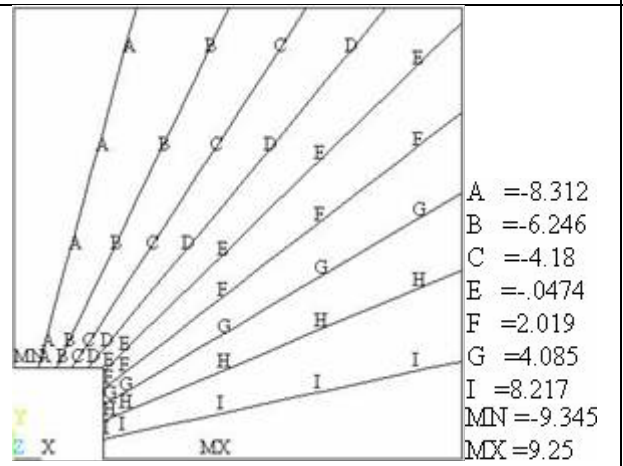

b) 120 °C

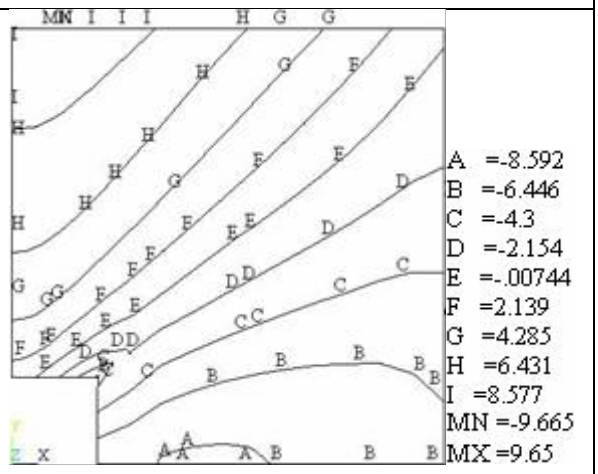

b) 120 °C, upper surface

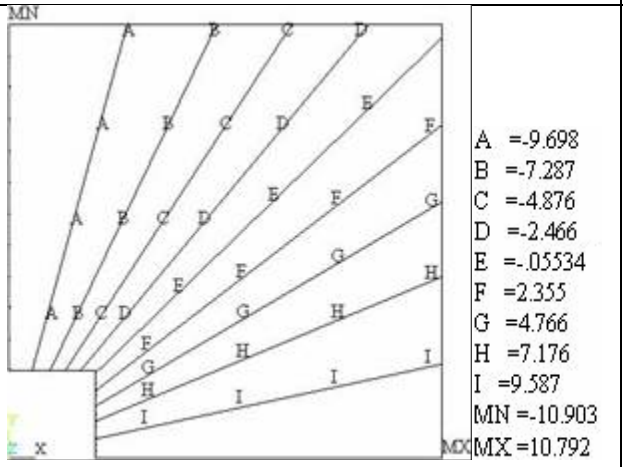

c) 140 °C

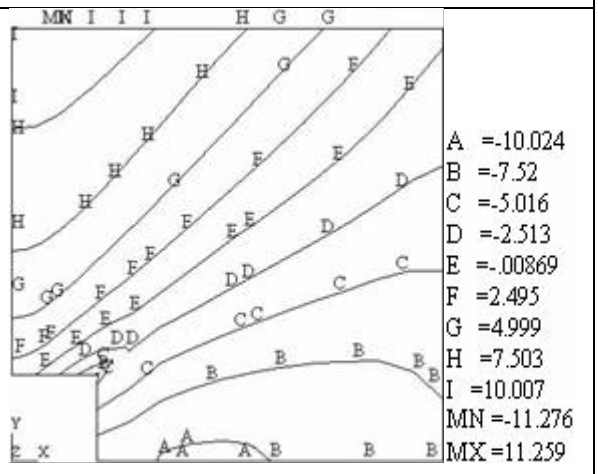

c) 140 °C, upper surface

A) Symmetric manner

B) Antisymmetric manner

Figure 5. Thermal stress distributions of symmetric and antisymmetric manners for x-direction at different thermal loadings (all stresses in MPa)

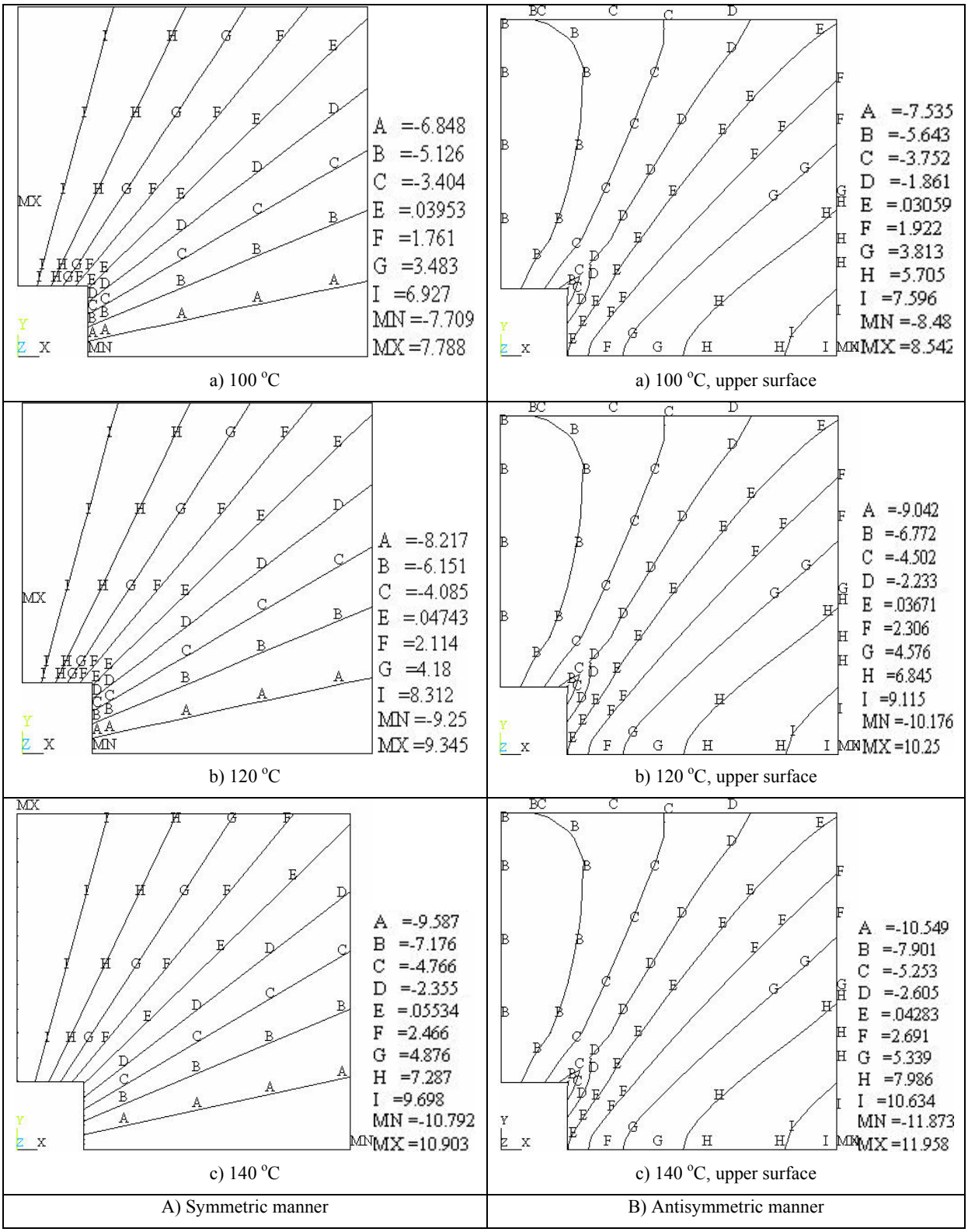

a) 100 °C | a) 100 °C, upper surface

b) 120 °C | b) 120 °C, upper surface

c) 140 °C | c) 140 °C, upper surface

A) Symmetric manner | B) Antisymmetric manner

Figure 6. Thermal stress distributions of symmetric and antisymmetric manners for y-direction at different thermal loadings (all stresses in MPa)

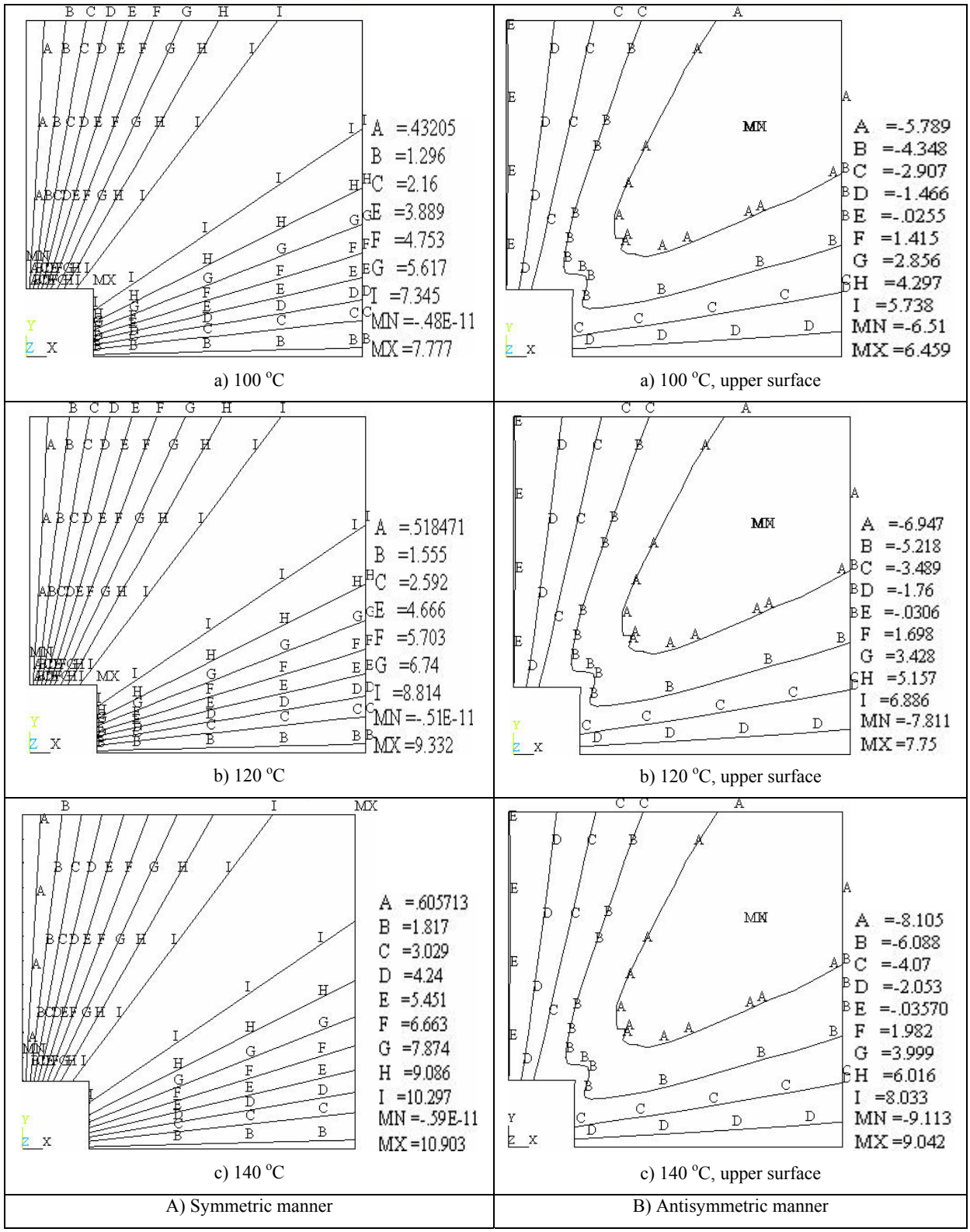

Figure 7. Thermal shear stress distributions of symmetric and antisymmetric manners at different thermal loadings (all stresses in MPa)

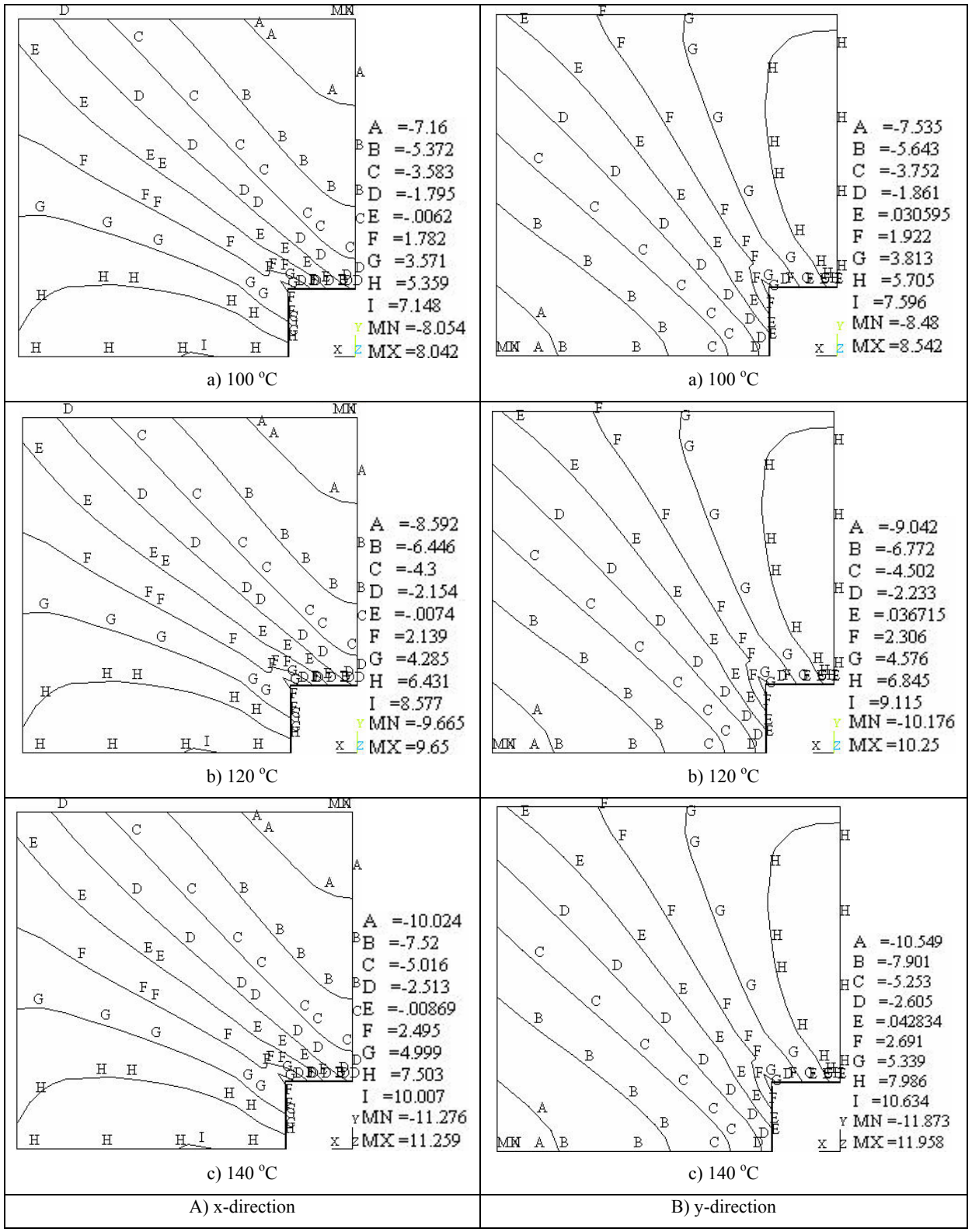

a) 100 °C

a) 100 °C

b) 120 °C

b) 120 °C

c) 140 °C

c) 140 °C

A) x-direction

B) y-direction

Figure 8. Thermal stress distributions on lower surface of antisymmetric manner at different thermal loadings (all stresses in MPa)